Hindawi
Journal of Chemistry
Volume 2020, Article ID 8653032, 6 pages
https://doi.org/10.1155/2020/8653032

Research Article

The Analysis of the Transformation Mechanism of cBN Crystals with the First-Principle Calculation

Lichao Cai,[1] **Bin Xu**,[1,2] **Meizhe Lv**,[2] **and Xiaohong Fan**[2]

[1]*School of Materials Science and Engineering, Shandong University, Jinan 250101, China*
[2]*School of Materials Science and Engineering, Shandong Jianzhu University, Jinan 250101, China*

Correspondence should be addressed to Bin Xu; xubin@sdjzu.edu.cn

Received 11 July 2020; Accepted 24 September 2020; Published 14 October 2020

Academic Editor: Tifeng Jiao

To clarify the synthesis mechanism of cubic boron nitride (cBN) with catalysts at high temperature and high pressure, we calculate the surface energy of the main phases in the Li-N-B synthesis system using the first-principle method. Based on the density functional theory, the surface energy of low-index surfaces of cBN, hexagonal boron nitride (hBN), and lithium boron nitride (Li_3BN_2) at the cBN synthetic temperature of 1700 K and synthetic pressure of 5.0 GPa is calculated. The surface energy of the main low-index surfaces of cBN is σ (111) > σ (001) > σ (110), that of hBN is σ $(10\bar{1}0) > \sigma$ $(11\bar{2}0) > \sigma$ (0001), and that of Li_3BN_2 is σ (100) > σ (110) > σ (001). The energy orders of the main low-index surfaces were well contrary to the corresponding orders of the valence electron density of the low-index surfaces of cBN, hBN, and Li_3BN_2, which were calculated by the empirical electron theory (EET) of solids and molecules. The result shows that the calculation results in this paper are well consistent with the previous results of the EET theory and support for the results of the "direct transformation of hBN to cBN under the catalysis of Li_3BN_2" obtained by the EET theory.

1. Introduction

Cubic boron nitride (cBN) single crystals have a high hardness value, high melting point, high thermal conductivity, wide energy gap, and low dielectric constant, which make them highly attractive as promising materials [1–4]. At present, cBN single crystals are synthesized using hexagonal boron nitride (hBN) as raw materials and lithium nitride (Li_3N) as catalysts by the static high-temperature and high-pressure (HPHT) catalytic method [5–7]. However, the present cBN single crystals still cannot meet the demand for advanced product development. The clear transformation mechanism of cBN crystals is significant to determine the quality of cBN crystals at HPHT. The research on the material surface and material catalysis mainly adopts the methods of characterization and theoretical research.

In our previous experimental study, the main phases are hBN, cBN, and Li_3BN_2 in the interface layers [8]. The empirical electron theory (EET) of solids and molecules has been successfully applied to the analysis of phase diagrams, phase transformation, and natural properties [9–11]. In the previous study, the transformation possibilities from hBN to cBN and from Li_3BN_2 to cBN were discussed with the valence electron structure [9]. However, the first-principle calculations based on the density functional theory became the most successful method and were applied widely in material calculations [12, 13]. The most stable surface of cBN crystals has been reported in detail using the CASTEP code [14, 15]. Meanwhile, the analysis about properties of (110) surfaces of cBN crystals has been discussed systematically [16]. The characters and properties of (111) and (100) of cBN crystals have also few reports in the previous studies [17, 18].

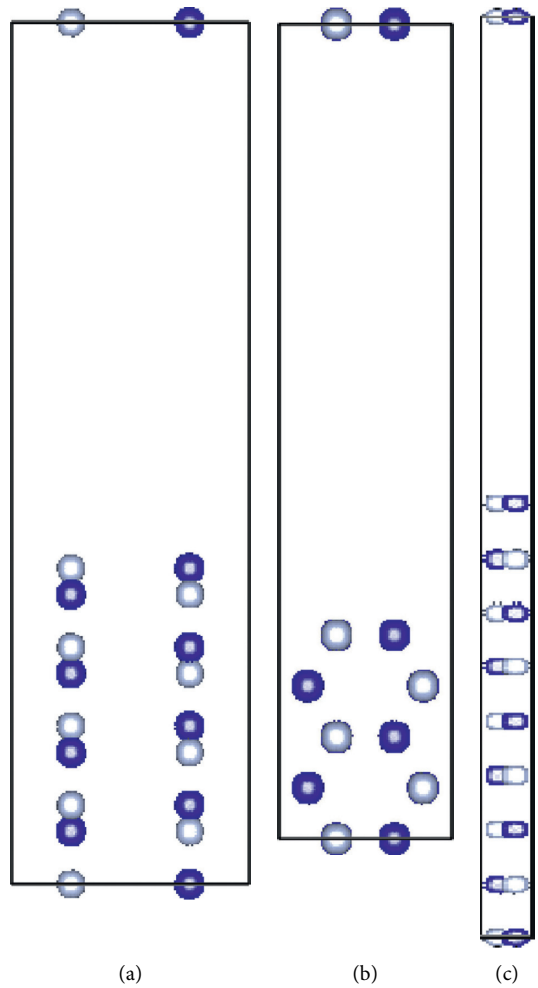

Figure 1: Schematic view of supercells for hBN along the <001> axis: (a) $(10\bar{1}\,0)$ slab with 9 layers, (b) $(11\bar{2}\,0)$ slab with 5 layers, and (c) (0001) slab with 9 layers. The gray and blue spheres represent B and N atoms, respectively.

However, the information of surfaces for hBN and Li_3BN_2 phases is barely referred in the previous studies. Thus, it is undoubtedly necessary to analyze the surface stability of three phases systematically, which helps understand the transformation mechanism of cBN crystals.

2. Materials and Methods

All calculations in the study were performed in the framework of the density functional theory using the VASP code (Vienna ab initio simulation program). The surface energies of lower-index surface planes on the three main phases, hBN, cBN, and Li_3BN_2, were calculated systematically [8]. An energy cutoff of 550 eV for the plane-wave basis was sufficient to obtain converged structural properties. Brillouin zone sampling was set with the $9 \times 9 \times 1$ k-point Monkhorst Pack grid meshes for all surfaces and with $9 \times 9 \times 3$, $9 \times 9 \times 9$, and $9 \times 9 \times 8$ k-points for hBN, cBN, and Li_3BN_2 bulks, respectively. For Perdew–Burke–Ernzerhof (PBE) calculations, the lattice constants used were as follows: $a = 2.505$ Å and $c = 6.601$ Å for hBN, $a = 3.615$ Å for cBN, and $a = 4.643$ Å and $c = 5.259$ Å for Li_3BN_2 [14, 15]. Symmetrically repeated slabs were adopted to avoid artificial charge transfer. After the convergence test, the slabs for cBN (100), (110), and (111) were created by 9, 9, and 13 layers, respectively; the slabs for hBN (0001), $(10\bar{1}0)$, and $(11\bar{2}0)$ were created by 9, 9, and 5 layers, respectively; and the slabs for Li_3BN_2 (001), (100), and (110) were created by 9, 15, and 11 layers, respectively. The models for hBN, cBN, and Li_3BN_2 with different layers are shown in Figure 1–3, respectively. A vacuum region of 15 Å for cBN, Li_3BN_2, and $(10\bar{1}0)$ and $(11\bar{2}0)$ of hBN and 30 Å for (0001) of hBN is adopted to prevent interactions between periodic images along the surface normal direction.

After structural relaxation, the surface energies (σ) [16, 17] of cBN, hBN, and Li_3BN_2 crystals were calculated as follows:

$$\sigma = \frac{(E_{\text{slab}} - E_{\text{bulk}})}{2A}, \tag{1}$$

where A is the area of the surface unit cell, E_{slab} is the total energy of the slab after relaxation, and E_{bulk} is the total energy of the crystals after relaxation. The main lower-index surfaces (100), (001), and (110) of Li_3BN_2 are polar with

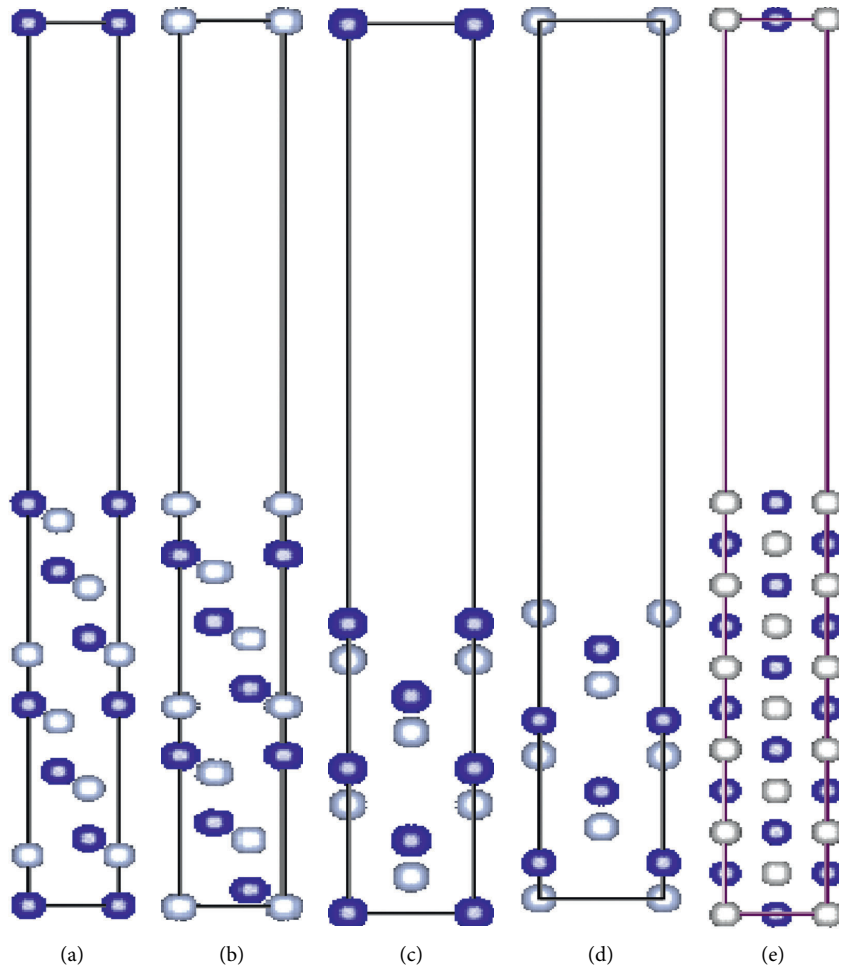

FIGURE 2: Schematic view of supercells for cBN along the <001> axis: (a) (111)-B slab with 13 layers, (b) (111)-N slab with 13 layers, (c) (100)-B slab with 9 layers, (d) (100)-N slab with 9 layers, and (e) (110) slab with 11 layers. The gray and blue spheres represent B and N atoms, respectively.

different types of B-, Li-, and N-terminated surfaces; however, their calculated surface energies were almost the same. Thus, the Li_3BN_2 surface energies of (100), (001), and (110) are defined by their average of the sum of all B-, Li-, and N- terminated surfaces, respectively. Five cBN schematic views for cBN single crystals can be obtained because of the polar surfaces of cBN (100) and (111), as shown in Figure 2, i.e., including (110), B- and N-terminated (100), and B- and N-terminated (111) surfaces. These surface energies (σ) [19, 20] of cBN single crystals can be calculated as follows:

$$\sigma = \frac{1}{2A}\left[E_{\text{slab}} - N_B\mu^{\text{bulk}} + (N_B - N_N)\mu_N^{\text{slab}}\right], \quad (2)$$

where N_B and N_N are the number of B and N atoms in the surface slab, respectively; $\mu^{\text{bluk}}$is the total energy of an atom in a bulk crystal at $T = 0$ K, and $\mu_N^{\text{slab}}$is the chemical potential of nitrogen.

3. Results

Figure 4 shows the surface energies of different cBN single-crystal models as a function of the N chemical potential in its allowed range. The calculated (110) surface energy was 0.175 eV/Å^2 in this work, which is in good agreement with the calculation results in [14–16]. Figure 4 shows that all lower surface energies of cBN single crystals are well consistent with those reported in previous theoretical studies [15]. The accuracy of the calculated cBN surface energy results ensures the validity of the calculation method used in the present study. For further analysis, the surface energies of cBN (111) and (100) are defined by the average surface energy of their B-terminated and N-terminated surfaces. Therefore, the main lower-index surface energies of cBN, hBN, and Li_3BN_2 at the cBN synthetic temperature of 1700 K and synthetic pressure of 5.0 GPa are obtained by the first-principle method.

The main average surface energies of the lower-index surfaces (100), (111), and (110) at 1700 K and 5.0 GPa for cBN are 0.475 eV/Å^2, 0.436 eV/Å^2, and 0.25 eV/Å^2, respectively. Thus, the order of the average lower-index surface energy of cBN at 1700 K and 5.0 GPa is σ (100) > σ (111) > σ (110). According to the previous EET study [9], valence electron density of surface (110) is greater than that of surfaces (111) and (100) at 1700 K and 5.0 GPa, so surface (110) of cBN is the most stable under this condition.

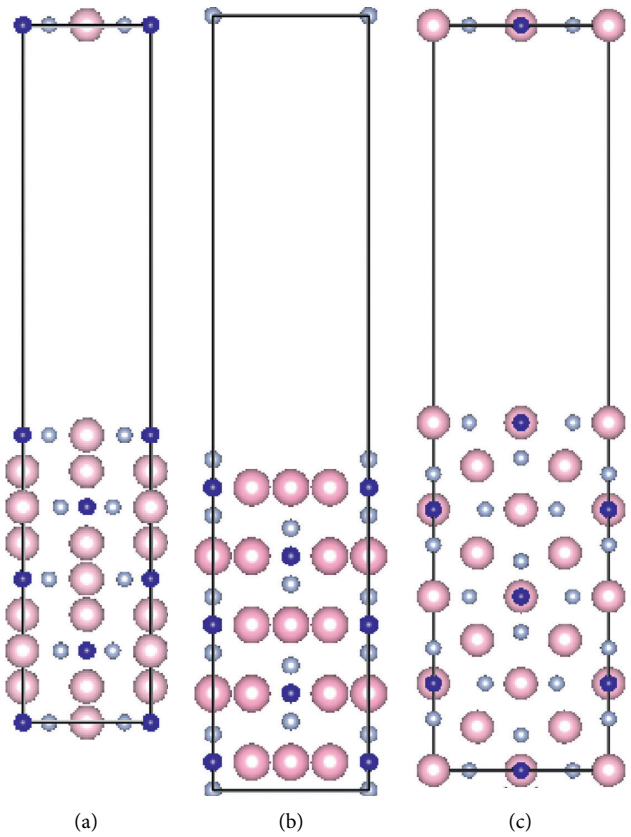

Figure 3: Schematic view of supercells for Li_3BN_2 along the <001> axis: (a) (001) slab with 9 layers, (b) (100) slab with 15 layers, and (c) (110) slab with 11 layers. The gray and blue spheres represent B and N atoms, respectively, and the big pink spheres represent Li atoms.

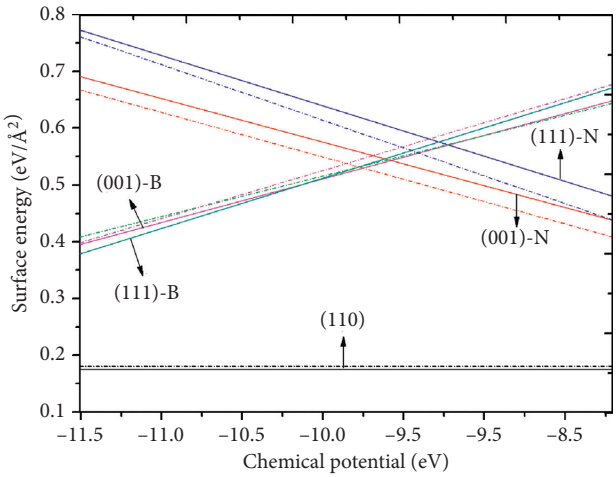

Figure 4: Surface energies of the three low-index cBN single-crystal surfaces as a function of the N chemical potential. The dashed line represents the theoretically calculated results obtained in [12].

Furthermore, the order of the valence electron density of cBN is $\rho\ (110) > \rho\ (111) > \rho\ (100)$ [6], which is completely contrary to the corresponding order of the surface energy of cBN. The higher the valence electron density, the smaller the surface energy and the more stable the surface. This means that the result of the cBN surface energy calculated by the first-principle theory well verifies the conclusion of the valence electron density calculated by the EET theory [9]. The surface energies of the main lower-index surfaces $(10\bar{1}0)$, $(11\bar{2}0)$, and (0001) at 1700 K and 5.0 GPa for hBN are 0.44 eV/Å^2, 0.22 eV/Å^2, and 0.02 eV/Å^2, respectively. It can be found that the order of the surface energy of hBN is as follows: $\sigma\ (10\bar{1}0) > \sigma\ (11\bar{2}0) > \sigma\ (0001)$. The main lower-index surfaces (100), (110), and (001) at 1700 K and 5.0 GPa

for Li_3BN_2 are 0.82 eV/Å^2, 0.33 eV/Å^2, and 0.25 eV/Å^2, respectively. Thus, the order of the surface energy of Li_3BN_2 is σ (100) > σ 110) > σ (001). Meanwhile, the order of the valence electron density of hBN and Li_3BN_2 at 1700 K and 5.0 GPa is ρ (0001) > ρ (11$\bar{2}$0) > ρ (10$\bar{1}$0) and ρ (001) > ρ (110) > ρ (100), respectively [9]. It could be concluded that the order of surface energies of hBN and Li_3BN_2 is also completely contrary to the corresponding order of the valence electron density of hBN and Li_3BN_2. Thus, the surface energies of hBN and Li_3BN_2 with the first-principle theory are well consistent with those results of the valence electron density by the EET theory. It could be concluded that the consistency between the first-principle theory for the surface energy and the EET theory for the valence electron density further confirms the credibility of the calculation results.

4. Discussion

Previous studies proved that the transformation possibilities from hBN to cBN are more than those from Li_3BN_2 to cBN at the cBN synthetic temperature of 1700 K and synthetic pressure of 5.0 GPa, and Li_3BN_2 could be the real catalyst in the synthesis process of cBN crystals [9, 21–23]. The surface energy of the catalyst could directly influence the nucleation rate. Among all values of the surface energy obtained so far, the surface energy of the (100) surface of Li_3BN_2 is the highest, i.e., 0.82 eV/Å^2, which is much greater than the other surface energies reported in this work. Thus, the nucleation of cBN crystals can easily occur around the (100) surface of Li_3BN_2; therefore, the catalyst material Li_3BN_2 using the (100) surface as the exposed surfaces could be used as substrates to induce effectively the growth of cBN single crystals.

5. Conclusions

The order of the main lower-index surface energies of cBN is σ (100) > σ (111) > σ (110); the order of the main lower-index surface energies of hBN is σ (10$\bar{1}$0) > σ (11$\bar{2}$0) > σ (0001); and the order of the main lower-index surface energies of Li_3BN_2 is σ (100) > σ (110) > σ (001). The orders of the surface energy of cBN, hBN, and Li_3BN_2 are all completely contrary to their corresponding orders of the valence electron density. Hence, the surface energies with the first-principle theory are well consistent with those results of the valence electron density by the EET. Comparing all surface energies in three phases (hBN, cBN, and Li_3BN_2), the (100) surface of Li_3BN_2 has the highest surface energy; therefore, it can be used as the substrate to induce effectively the growth of cBN crystals.

Data Availability

The data used to support the findings of this study are included within the article.

Conflicts of Interest

The authors declare no conflicts of interest.

Authors' Contributions

Lichao Cai contributed to data curation and wrote the original draft; Bin Xu was involved in funding acquisition and supervised the study; Meizhe Lv and Xiaohong Fan investigated the study; Xiaohong Fan contributed to methodology; and Meizhe Lv contributed to writing, reviewing, and editing.

Acknowledgments

This work was financially supported by the National Natural Science Foundation of China (Grant no. 51272139).

References

[1] W. Ding, B. Linke, Y. Zhu et al., "Review on monolayer CBN superabrasive wheels for grinding metallic materials," *Chinese Journal of Aeronautics*, vol. 30, no. 1, pp. 109–134, 2017.

[2] X. W. Zhang, "Doping and electrical properties of cubic boron nitride thin films: a critical review," *Thin Solid Films*, vol. 544, pp. 2–12, 2013.

[3] R. Mohammad and Ş. Katırcıoğlu, "The structural and electronic properties of BAs and BP compounds and BPxAs1−x alloys," *Journal of Alloys and Compounds*, vol. 485, no. 1-2, pp. 687–694, 2009.

[4] X. L. Yuan, J. Niitsuma, T. Sekiguchi, M. Takase, and T. Taniguchi, "Characterization of p-n junction formed at the boundary of facets in cubic-BN using scanning electron microscope," *Diamond and Related Materials*, vol. 14, no. 11-12, pp. 1955–1959, 2005.

[5] S. Nakano, H. Ikawa, and O. Fukunaga, "Synthesis of cubic boron nitride using Li_3BN_2, $Sr_3B_2N_4$ and $Ca_3B_2N_4$ as solvent-catalysts," *Diamond and Related Materials*, vol. 3, no. 1-2, pp. 75–82, 1994.

[6] O. Fukunaga and S. Takeuchi, "Growth mechanism of cubic BN using Li_3BN_2 solvent under high pressure," *International Journal of Refractory Metals and Hard Materials*, vol. 55, pp. 54–57, 2016.

[7] Y. Du, Z. Su, D. Yang et al., "Synthesis of black cBN single crystal in hBN-Li_3N-B system," *Materials Letters*, vol. 61, no. 16, pp. 3409–3412, 2007.

[8] S. Li, X. F. Guo, B. Xu, and H. Wang, "Fracture morphology and XRD layered characterization of cBN cake," *Journal of Synthetic Crystals*, vol. 41, no. 1, pp. 15–19, 2012.

[9] M.-Z. Lv, B. Xu, L.-C. Cai, F. Jia, and X.-D. Yuan, "Analysis of transition mechanism of cubic boron nitride single crystals under high pressure-high temperature with valence electron structure calculation," *Chinese Physics Letters*, vol. 36, no. 1, Article ID 013101, 2019.

[10] C. Lin, G. Yin, Y. Zhao, and J. Wang, "Analysis of the effect of alloy elements on allotropic transformation in titanium alloys with the use of cohesive energy," *Computational Materials Science*, vol. 111, pp. 41–46, 2016.

[11] C. Lin, G. Yin, A. Zhang, Y. Zhao, and Q. Li, "Simple models to account for the formation and decomposition of athermal ω phase in titanium alloys," *Scripta Materialia*, vol. 117, pp. 28–31, 2016.

[12] H. Liu, Q. Li, L. Zhu, and Y. Ma, "Superhard and superconductive polymorphs of diamond-like BC3," *Physics Letters A*, vol. 375, no. 3, pp. 771–774, 2011.

[13] S. N. Shirodkar and E. Kaxiras, "Li Intercalation at graphene/hexagonal boron nitride interfaces," *Physical Review B*, vol. 93, no. 24, 2016.

[14] H. Ruuska and K. Larsson, "Surface reactivities of (111), (100), and (110) planes of c-BN: a quantum mechanical approach," *Diamond and Related Materials*, vol. 16, no. 1, pp. 118–123, 2007.

[15] N. Wang, L. Dong, M. S. Li, and D. J. Li, "Comparison and stability of the low-index surfaces of c-BN by first-principles," *Vacuum*, vol. 104, pp. 92–96, 2014.

[16] N. Ooi and J. B. Adams, "Ab initio studies of the cubic boron nitride (110) surface," *Surface Science*, vol. 574, no. 2-3, pp. 269–286, 2005.

[17] F. Hui, P. Vajha, Y. Ji et al., "Variability of graphene devices fabricated using graphene inks: atomic force microscope tips," *Surface and Coatings Technology*, vol. 320, pp. 391–395, 2017.

[18] B. Xu, M. Lv, X. Fan, W. Zhang, Y. Xu, and T. Zhai, "Lattice parameters of hexagonal and cubic boron nitrides at high temperature and high pressure," *Integrated Ferroelectrics*, vol. 162, no. 1, pp. 85–93, 2015.

[19] H. Yamane, S. Kikkawa, and M. Koizumi, "High- and low-temperature phases of lithium boron nitride, Li_3BN_2: preparation, phase relation, crystal structure, and ionic conductivity," *Journal of Solid State Chemistry*, vol. 71, no. 1, 11 pages, 1987.

[20] T. D. Beaudet, J. R. Smith, and J. W. Adams, "Surface energy and relaxation in boron carbide $(10\bar{1}1)$ from first principles," *Solid State Communications*, vol. 219, no. C, pp. 43–47, 2015.

[21] M. Lv, B. Xu, L. Cai, X. Guo, and X. Yuan, "Auger electron spectroscopy analysis for growth interface of cubic boron nitride single crystals synthesized under high pressure and high temperature," *Applied Surface Science*, vol. 439, pp. 780–783, 2018.

[22] X. Guo, B. Xu, W. Zhang, Z. Cai, and Z. Wen, "XPS analysis for cubic boron nitride crystal synthesized under high pressure and high temperature using Li_3N as catalysis," *Applied Surface Science*, vol. 321, pp. 94–97, 2014.

[23] M. Lv, B. Xu, X. Guo, L. Cai, and X. Yuan, "Electron energy loss spectroscopy analysis for cubic boron nitride single crystals transition mechanism in Li_3N-BN system," *Materials Letters*, vol. 242, pp. 75–78, 2019.